



1

2 Novel β subunit mutation causes a slow-channel syndrome by 3 enhancing activation and decreasing the rate of agonist dissociation

4 Manuel F. Navedo,^a José A. Lasalde-Dominicci,^b Carlos A. Báez-Pagán,^b Luzed Díaz-Pérez,^b
 5 Legier V. Rojas,^c Ricardo A. Maselli,^d Julie Staub,^e Kelly Schott,^e
 6 Roberto Zayas,^e and Christopher M. Gomez^{e,*}

7 ^aDepartment of Physiology and Biophysics, University of Washington, Seattle, WA 98195-7290, USA

8 ^bDepartment of Biology, University of Puerto Rico, San Juan, PR 00931, USA

9 ^cDepartment of Physiology, Universidad Central del Caribe, Bayamón, PR 00960, USA

10 ^dSection of Neuroscience, University of California, Davis, CA 95616, USA

11 ^eDepartment of Neurology and Neuroscience, MMC 295 420 Delaware St. SE University of Minnesota, Minneapolis, MN 55455, USA

12 Received 5 October 2005; revised 8 February 2006; accepted 21 February 2006

13

14

15 We traced the cause of a slow-channel syndrome (SCS) in a patient
 16 with progressive muscle weakness, repetitive compound muscle action
 17 potential and prolonged low amplitude synaptic currents to a V → F
 18 substitution in the M1 domain of the β subunit (β V229F) of the muscle
 19 acetylcholine receptor (AChR). In vitro expression studies in *Xenopus*
 20 oocytes indicated that the novel mutation β V229F expressed normal
 21 amounts of AChRs and decreased the ACh EC₅₀ by 10-fold compared
 22 to wild type. Kinetic analysis indicated that the mutation displayed
 23 prolonged mean open duration and repeated openings during activa-
 24 tion. Prolonged openings caused by the β V229F mutation were due to a
 25 reduction in the channel closing rate and an increase in the effective
 26 channel opening rate. Repeated openings of the channel during
 27 activation were caused by a significant reduction in the agonist
 28 dissociation constant. In addition, the β V229F mutation produced an
 29 increase in calcium permeability. The kinetic and permeation studies
 30 presented in this work are sufficient to explain the consequences of the
 31 β V229F mutation on the miniature endplate currents and thus are
 32 direct evidence that the β V229F mutation is responsible for compro-
 33 mising the safety margin of neuromuscular transmission in the patient.
 34 © 2006 Published by Elsevier Inc.

35
36

Introduction

37 The slow-channel syndrome (SCS) is a disorder characterized
 38 by muscular weakness and fatigability due to gain-in-function
 39 mutations in the subunits of the muscle acetylcholine receptor
 40 (AChR) of the neuromuscular junction (NMJ). SCS-associated
 41 mutations dramatically alter the function of the AChRs and thus

impair neuromuscular transmission (Engel et al., 1996; Muley 42
 and Gomez, 2002). Characterization of the kinetic abnormalities 43
 produced by the SCS-associated mutations has provided 44
 insightful information about the consequences of the mutations 45
 on synaptic transmission and into the structure and function of 46
 the AChR. 47

Several molecular mechanisms underlying the SCS have been 48
 identified. For example, SCS mutations in the extracellular domain 49
 of the α subunit, which forms the presumed ligand binding pocket, 50
 cause increased ACh affinity leading to repeated openings of the 51
 channel during activation and to a slower decay of the synaptic 52
 current (Sine et al., 1995; Croxen et al., 1997). Numerous SCS 53
 mutations in the M2 domain, which line the water-filled ion channel 54
 pore, have a pronounced effect on ion channel gating (closing and 55
 opening rate constants), causing prolongation of single-channel 56
 open times, of activation episodes and, as a consequence, of 57
 synaptic decay phases (Milone et al., 1997; Gomez et al., 2002b; for 58
 a review, see Engel et al., 2003). More recently, SCS mutations in 59
 the M1 domain of the α and ϵ subunits were found to slow the rate 60
 of agonist unbinding, resulting in an increase in the number of re- 61
 openings per activation episode and prolonged activation events 62
 (Wang et al., 1997; Hatton et al., 2003). This kinetic abnormality 63
 was enough to explain the prolonged decay time of the synaptic 64
 current observed in the patients. These results indicated a 65
 modulatory role of the M1 domain in structures that couple ligand 66
 binding to the channel gate. 67

Here, we described a novel form of SCS cause by a β V229F 68
 mutation in the M1 domain of the AChR β subunit. In vitro 69
 expression studies in *Xenopus* oocytes indicated that the β V229F 70
 mutation did not affect expression levels of the receptor, but 71
 significantly increased the duration of the channel opening 72
 episodes. Kinetic analysis revealed that the prolonged open 73
 channel episodes were the result of a significant reduction in the 74

* Corresponding author.

E-mail address: gomez001@tc.umn.edu (C.M. Gomez).

Available online on ScienceDirect (www.sciencedirect.com).

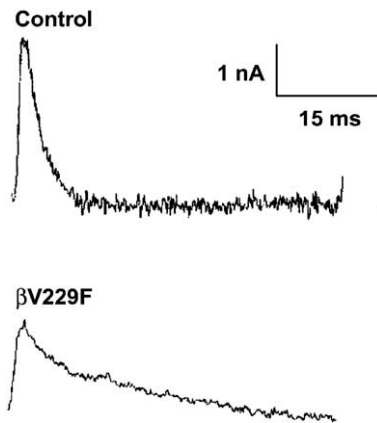


Fig. 1. Electrophysiological studies. Miniature endplate currents (MEPC) recorded from the anconeus muscle of control and the proband UM:III4. The prolonged miniature endplate current (MEPC) has a bi-exponential decay time constant of 2.3 ms and 26.1 ms, compared with control (3.6 ms).

75 agonist dissociation and closing rates constants, combined with an
76 increase in the effective opening rate of the channel. This indicated
77 a contribution of position β V229 to channel gating and an apparent
78 allosteric modulation of the binding site. These observations are
79 somewhat unexpected since other SCS-M1 domain mutations
80 mainly affect the agonist dissociation constant with little or no
81 effect on the other time constants. Nevertheless, the kinetic and
82 permeation studies presented in this study are direct and irrefutable
83 evidence indicating that the β V229F mutation is responsible for
84 compromising the safety margin of neuromuscular transmission in
85 the patient.

86 Results

87 Clinical and electrophysiological studies

88 The proband of Kindred UM7 (Fig. 2A) was a 75-year-old
89 male (UM7:II3) who noted slowly progressive weakness and later
90 atrophy of hand and forearm muscles in his teens, leg weakness
91 in his 60s and neck weakness at 70. His mother and two uncles
92 (UM7:I2–I4) had similar symptoms. His niece (UM7:III1) had
93 intermittent weakness since her teens and developed slowly
94 progressive hand weakness in her 40s. Two sons, one asymp-
95 tomatic at age 53 (UM7:III3) and one with forearm weakness
96 since age 50 (UM7:III4), had mild eye muscle weakness when
97 examined. Compound muscle action potentials recorded in hand
98 or forelimb muscles showed hallmark repetitive responses to
99 single stimuli and evidence of impaired neuromuscular transmis-
100 sion in the proband, two of his sons and his niece, suggesting the
101 presence of a dominantly inherited congenital myasthenic
102 syndrome. In vitro microelectrode studies performed on the left
103 anconeus muscle of the proband's son (UM:III4) at age 48
104 revealed that the quantal release by the nerve impulse was
105 reduced by 40%. In addition, the amplitude of the miniature
106 endplate current (MEPC) was reduced by 61% and MEPC were
107 prolonged and decayed bi-exponentially, with one open time
108 component close to normal and one significantly prolonged (Fig.
109 1; Table 1). These results suggested a severe reduction in safety
110 factor of neuromuscular transmission caused by a kinetic disorder
111 of the AChR. These characteristics were not observed in 82
112 individuals used as control.

Genetic studies

We identified a G-to-T transversion at position 770 of the β
subunit gene coding region, predicting the missense mutation
 β V229F, in genomic DNA from affected members of this kindred
(Fig. 2B). Patient 7-1, two of his sons, his niece and one of her
sons were heterozygous for this mutation (Fig. 2A). His third son
and one great nephew, who had no neuromuscular symptoms, only
had the normal sequence (Fig. 2C). Moreover, using allele-specific
PCR to specifically detect either the mutant or wild-type sequence
for position β 770G/T, we confirmed that this mutation was absent
in a panel of 100 unrelated human control genomic DNA samples.
Additional sequence changes, ϵ C530T and ϵ C1304T, identified in

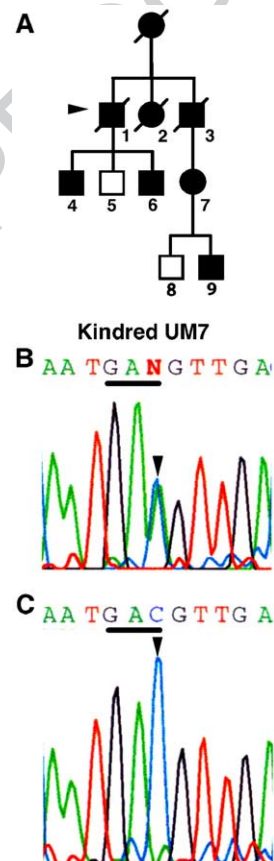


Fig. 2. Mutations in one kindred with slow-channel syndrome affect a β subunit residues. (A) Pedigree of kindred UM7. Proband 7-1 (arrowhead), his sons, 7-4, 7-6, and niece 7-7 had abnormal electrodiagnostic studies. (B) Genomic sequence of the β subunit encoding the region of the M1 domain complementary strand, nucleotides 765–775, containing the nucleotide position affected in kindred 7. The colored single-letter codes above show the letter N at position 770, where the sequence indicates two nucleotides. Shown is sequence from patient 7-6. One of the parental strands contains a C-to-A (antisense of G-to-T, arrowhead) substitution, which is present in equivalent abundance to the normal C and which alters the codon GTC to TTC. This mutation occurs at codon V229 and predicts a substitution of a phenylalanine residue. The complementary sequence of codon 229 is underlined. The larger black letters are letter codes for the corresponding amino acids and indicate the position encoding the wild type, valine (V), together with the mutant phenylalanine (F), read in the reverse sequence of the complementary strand. (C) Sequence of the same region obtained from the patient's normal cousin (7-8) containing only a nucleotide C and amino acid valine at this position.

t1.1 Table 1
Serial microelectrode studies of neuromuscular transmission in the slow-channel syndrome

Measurements	Control	UM:III4
t1.4 MEPP amplitude (mV)	0.8 ± 0.04 (n = 82)	0.7 ± 0.3 (n = 16)
t1.5 EPP QC (1 Hz)	22.6 ± 3.0 (n = 16)	13.8 ± 4.8 (n = 14)
t1.6 MEPC amplitude (nA)	4.6 ± 0.3 (n = 11)	1.8 ± 0.4 (n = 6)
t1.7 MEPC decay time	3.6 ± 0.2 (n = 11)	$\tau_1 = 2.3 \pm 1.4$ (n = 6)
t1.8 constant (ms)		$\tau_2 = 26.1 \pm 5.0$ (n = 6)
t1.9 MEPC frequency		6.4 ± 4.4 (n = 10)

t1.10 Values are given as mean ± SEM. Numbers in parenthesis indicate numbers of EP examined.

125 patient 7-1 that did not lead to a change in amino acid sequence or
126 affect splice sites were considered genetic polymorphisms.
127 Table 2 compares the amino acid sequence for several M1
128 domains in the region containing the β V229F mutation. It
129 demonstrates that the β V229F mutation occurs in an amino acid
130 residue that is highly conserved in all β subunits of all vertebrate
131 species studied and conserved or substituted conservatively
132 between numerous M1 domains in several nicotinic subunits in
133 other species. This observation indicates that this position may be
134 important for proper channel function.

135 *Functional consequences of the β V229F mutations on the*
136 *macroscopic response*

137 Dose–response curves were generated to determine the overall
138 consequences of the β V229F mutation (Fig. 3). The dose–
139 response curve for the β V229F mutant was shifted to lower ACh
140 concentrations, with a 10-fold reduction in EC_{50} (5.5 μ M) as
141 compared to wild type (54 μ M). In addition, we observed a 3.6-
142 fold increase in the normalized macroscopic response for the
143 β V229F mutant (Table 3). The Hill coefficient was not affected by
144 the β V229F mutation, suggesting that the mutation affects channel
145 function without affecting channel cooperativity. Binding of [¹²⁵I]
146 α -bungarotoxin to surface receptors showed no changes in AChR

t2.1 Table 2
t2.2 Multiple alignment sequences of the AChR M1 domain

Human subunits M1 domain				
t2.4	α 1	PLFYIVN	V	IIPCLLSFSLTGLVFYLP
t2.5	β 1	PLFYLVN	V	IAPCILTLLAIFVFYLP
t2.6	δ	PLFYIIN	I	LVPCLVISFMVNLVFLPA
t2.7	ϵ	PLFYVIN	I	IVPCVLISGLVLLAYFLPA
t2.8	α 2	PLFYTIN	L	IIPCLLSISCLTVLVFYLP
t2.9	α 3	PLFYTIN	L	IIPCLLSISCLTVLVFYLP
t2.10	α 4	PLFYTIN	L	IIPCLLSISCLTVLVFYLP
t2.11	α 7	TLYYGLN	L	LIPCVLISALALLVFLPA
t2.12	β 2	PLFYTIN	L	IIPCVLITSLAILVFLYLP
t2.13	β 4	PLFYTIN	L	IIPCVLITLLAILVFLYLP
t2.14	β 1	PLFYLVN	V	IAPCILTLLAIFVFYLP
t2.15	Patient		F	
<i>β1 subunits M1 domain</i>				
t2.18	<i>Xenopus</i>	PLFYIVN	V	IVPCILITILAIFVFYLP
t2.19	Mouse	PLFYLVN	V	IAPCILTLLAIFVFYLP
t2.20	Rat	PLFYLVN	V	IAPCILTLLAIFVFYLP
t2.21	Bovine	PLFYLVN	V	IAPCILTLLAIFVFYLP
t2.22	Human	PLFYLVN	V	IAPCILTLLAIFVFYLP
t2.23	Patient		F	

expression produced by the β V229F mutation (Table 3), indicating
normal assembly and oligomerization of the β V229F AChR.

Single-channel studies

To investigate the molecular basis and mechanistic consequence of the β V229F mutation, we recorded single-channel currents in the cell-attached configuration at -100 mV and 4μ M ACh from oocytes expressing wild-type and β V229F AChRs (Fig. 4). Table 4 summarizes the single-channel parameters obtained for the AChRs studied. Single-channel currents elicited at 4μ M ACh demonstrated that the mutation β V229F significantly increased the channel mean open time constant (11.4 ms) and mean burst duration (20.7 ms) as compared to wild type (Fig. 4 and Table 4). Single-channel amplitude was similar for wild-type (wt) and β V229F AChRs (Fig. 4; Table 4).

To interpret the kinetic behavior of wt and mutant AChRs, we used a simple kinetic model with two open states (see Experimental methods). Fig. 5 shows records of individual bursts and their respective mean open and closed time distribution histograms at 100μ M ACh. We found that, at 100μ M ACh, the β V229F mutation decreased the diliganded closing rate (α_2 , 1200) and significantly increased the effective opening rate ($\beta_2 = 33,500 \text{ s}^{-1}$)

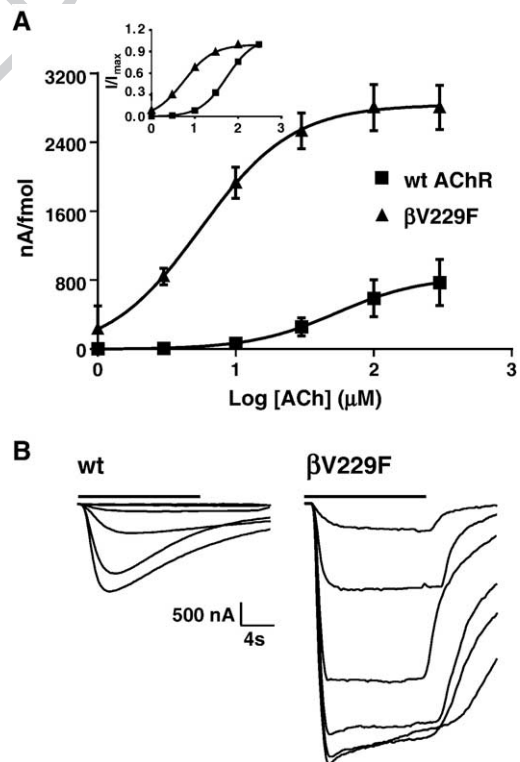


Fig. 3. Functional consequences of wild-type and β V229F AChR expressed in *Xenopus* oocytes. (A) Dose–response curves from muscle wild-type and β V229F voltage-clamped oocytes. Peak for individual oocytes was obtained from ACh-induced current at 1, 3, 10, 30, 100 and 300 μ M ACh. The values at each concentration were averaged, and dose–response curves were reconstructed and normalized to nA per fmol. Inset represents dose–response curves for each of the AChRs tested normalized to maximal response. (B) Representative inward current traces showing normalized ACh-induced current from wild-type and the β V229F mutation. Bars on top of the macroscopic currents traces represent ACh application. The estimated parameters of the fitted curves are summarized in Table 3.

t3.1 Table 3

t3.2 Functional consequences of SCCMS mutations

t3.3	AChR type ($\alpha\beta\delta\epsilon$)	Expression level (fmol)	EC ₅₀ (μ M)	Hill coefficient	Normalized response ($-nA/fmol$)
t3.4	Wild type	2.3 \pm 0.5	54 \pm 1	1.4 \pm 0.5	800 \pm 300
t3.5	β V229F	1.4 \pm 0.4	5.5 \pm 1*	1.3 \pm 0.5	2800 \pm 700*

t3.6 Values are given as the mean \pm SEM. Normalized peak channel activity for individual oocytes was obtained by dividing the ACh-induced current at 300 μ M by the fmol of AChR expressed on each oocyte. AChR expression levels, EC₅₀, Hill coefficients and normalized responses were calculated using 7–13 oocytes.

t3.7 * $P < 0.05$.

168 as compared to wild-type receptors (19,000 s⁻¹; Table 5). These
 169 changes produced an increase in the effective diliganded open
 170 channel equilibrium constants estimated at 100 μ M ACh (Θ_2) from
 171 11 in wild-type AChRs to 28 in β V229F AChRs. In addition, we
 172 observed a significant reduction in the agonist dissociation constant
 173 (700 s⁻¹) as compared to wild type (3600 s⁻¹, Table 5). These
 174 results explain the increase in the number of openings per
 175 activation episodes from 3 in wild-type to 11 in the β V229F
 176 mutation (Figs. 4 and 5). The kinetic analysis of single-channels
 177 demonstrated that the greatly prolonged MEPC decay phases
 178 recorded in muscle from patient 7-2 can be explained on a
 179 molecular level. The perturbed function in β V229F AChRs and, as
 180 a consequence, the prolonged MEPC in the patient are due to an
 181 increase in the burst length and number of openings per activation
 182 episode caused by a reduction in the diliganded closing rate and
 183 agonist dissociation constant and an increase diliganded effective
 184 opening rate constant (Table 5).

185 *Calcium permeability*

186 Some M1 and M2 domain residues may line the channel pore and
 187 determine permeability. To determine if the permeability of the Ca²⁺
 188 was changed in this mutation, we applied the Goldman–Hodgkin–
 189 Katz (GHK) constant field model to obtain the permeability ratios

from current reversal potentials (Castro and Albuquerque, 1995; 190
 Cens et al., 1997). The reversal potentials for wild-type and the 191
 mutant receptor were calculated from recordings made with 192
 solutions containing a 1 mM and 10 mM Ca²⁺ concentrations. 193
 Current–voltage relationships were used to determine the reversal 194
 potentials in different solutions (Fig. 6). The relative permeability 195
 value of Ca²⁺ with respect to cesium (P_{Ca}/P_{Cs}) in wild-type 196
 receptor was 0.37 \pm 0.24 ($n = 4$) which is very similar to values 197
 previously reported (Castro and Albuquerque, 1995). The β V229F 198
 mutation, however, produced a significant increase in P_{Ca}/P_{Cs} (1.56 199
 \pm 0.41) as compared to wild type (0.37 \pm 0.24; $P < 0.001$, $n = 6$; Fig. 200
 6). This greater than 4-fold increase in the preference of the receptor 201
 for using Ca²⁺ as a charge carrier correlates well with the marked 202
 endplate myopathy seen in this patient. Functionally, the increase in 203
 calcium permeability indicates that the β V229F mutation not only 204
 contributes to the formation of the pore, but also is involved in 205
 determining the ion selectivity of the channel. 206

207 **Discussion**

208 In the SCS, weakness associated with impaired neuromuscular 209
 transmission and prolonged synaptic currents has been attributed to 210
 a variety of mutations in different domains of the four subunits 211

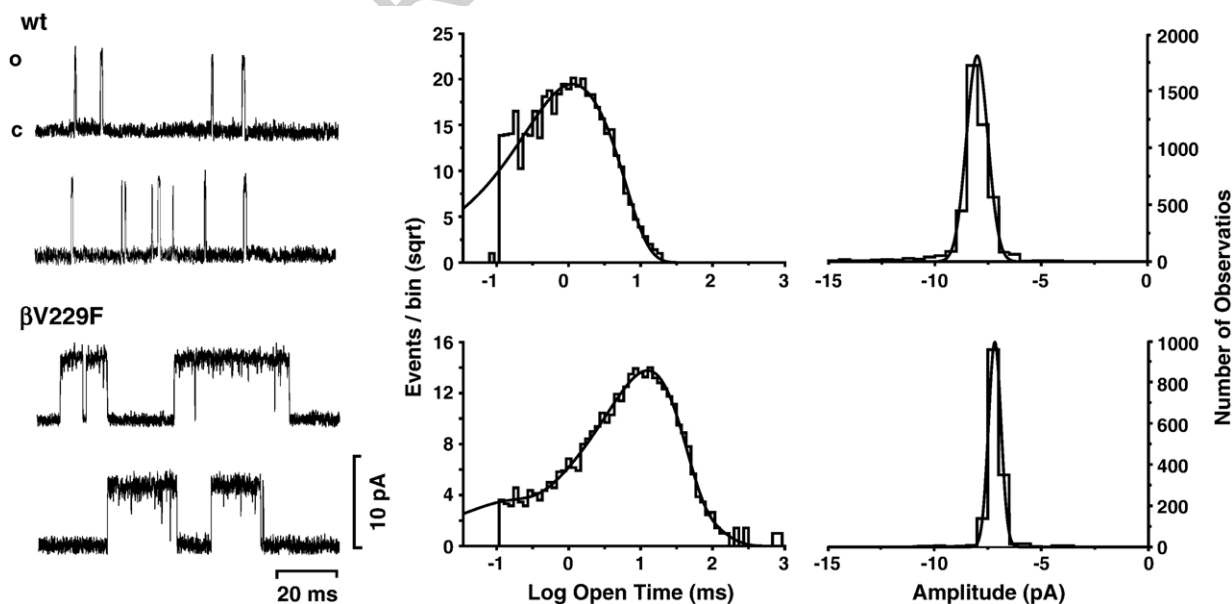


Fig. 4. Single-channel currents for wild type and β V229F elicited by 4 μ M ACh. Currents were recorded from *Xenopus* oocytes expressing either wild-type or the mutant AChRs, as indicated. Center panel, open duration histograms corresponding to the AChRs studied were fitted with exponential functions of the appropriate number of components using the maximum likelihood algorithm. Data were filtered at 5 kHz for each current sample displayed, and channel openings are shown as upward deflections (left panel). Right panel: amplitude histograms. Both wt and mutant AChR show a single amplitude component. All channels were recorded at a holding potential of -100 mV, a sampling rate of 50 kHz and at a temperature of 22°C. Calculated parameters are summarized in Table 4.

t4.1 Table 4
t4.2 Single-channel recording of wt and mutant AChRs expressed in *Xenopus* oocytes

t4.3	AChR	[ACh] (μM)	Patches/events ^a	τ_{o1} (ms)	Fraction	τ_{o2} (ms)	Fraction	σ (pA)	τ_B (ms)
t4.4	wt	4	3/6996	0.591	0.335	1.59	0.665	7.9 ± 1.0	2.60 (0.68)
t4.5	βV229F	4	14/3420	0.092	0.038	11.4	0.925	7.2 ± 0.3	20.7 (0.92)

t4.6 Single-channel currents were recorded in cell-attached patches at a holding potential of -100 mV, temperature at 22°C and at a sampling rate of 50 kHz.

t4.7 ^a Number of patches/number of events. σ represent AChR single-channel amplitude in pA. τ_B represents mean burst duration.

211 forming the muscle AChR (Gomez and Gammack, 1995; Ohno et
212 al., 1995; Sine et al., 1995; Engel et al., 1996; Gomez et al., 1996;
213 Croxen et al., 1997; Milone et al., 1997; Gomez et al., 1998;
214 Croxen et al., 2002; Gomez et al., 2002a). In the present study, we
215 provided the first description of an SCS-associated mutation in the
216 M1 domain of the AChR β subunit. The patient and several
217 members of his family showed slowly progressive muscular
218 weakness. In addition, endplate myopathy was marked by
219 extensive remodeling of the neuromuscular junction (data not
220 shown). In vitro microelectrode studies revealed prolonged low
221 amplitude MEPC in the patient. The clinical and electrophysio-
222 logical outcomes of the SCS were traced to a kinetic disorder of the
223 AChR attributed to a novel gain-of-function mutation, βV229F , in
224 the M1 domain of the β subunit. Thus, the safety factor for
225 neuromuscular transmission is compromised by a prolonged low
226 amplitude synaptic current resulting from abnormally prolonged
227 single-channel activation episodes.

228 In vitro expression studies in *Xenopus* oocytes combined with
229 kinetic analysis provided a mechanistic explanation for the
230 consequences of the mutation on the synaptic current. First, we
231 observed that, in whole-cell experiments, mutation βV229F shifted
232 to the left the ACh EC_{50} , when compared to wild type (Table 3).
233 This result, even though indirect (Colquhoun, 1998; Burzomato et

234 al., 2004), suggested that mutation βV229F increased the open
235 probability of the channel. Single-channel analysis at low ACh
236 concentration confirmed our hypothesis. At low ACh concentra-
237 tion, mutation βV229F significantly increases the channel mean
238 open time and, more importantly, the mean burst duration. Kinetic
239 analysis revealed that the gain-in-function produced by mutation
240 βV229F could be explained by a 5-fold reduction in the agonist
241 dissociation constant from the diliganded channel, a decrease in the
242 diliganded closing rate and a 2-fold increase in the effective
243 opening rate compared to wild type. These changes are responsible
244 for an increase in the number of opening per activation episode and
245 the 2.4-fold increase in the effective diliganded open channel
246 equilibrium (Θ_2) in βV229F AChRs.

247 In SCS, the reduced safety margin of neuromuscular transmis-
248 sion and neuromuscular weakness results from several structural
249 and functional factors that are mostly the consequence of the
250 prolonged synaptic currents. The immediate cause of the prolonged
251 MEPCs is that, during neuromuscular transmission, most AChRs
252 will immediately bind two ACh molecules, and the decay time
253 constant of the MEPC will be approximately determined by the
254 slow component of the burst length distribution at low ACh
255 concentrations. Our analysis indicated that the 5-fold increase in
256 the agonist dissociation constant, the reduction in the channel

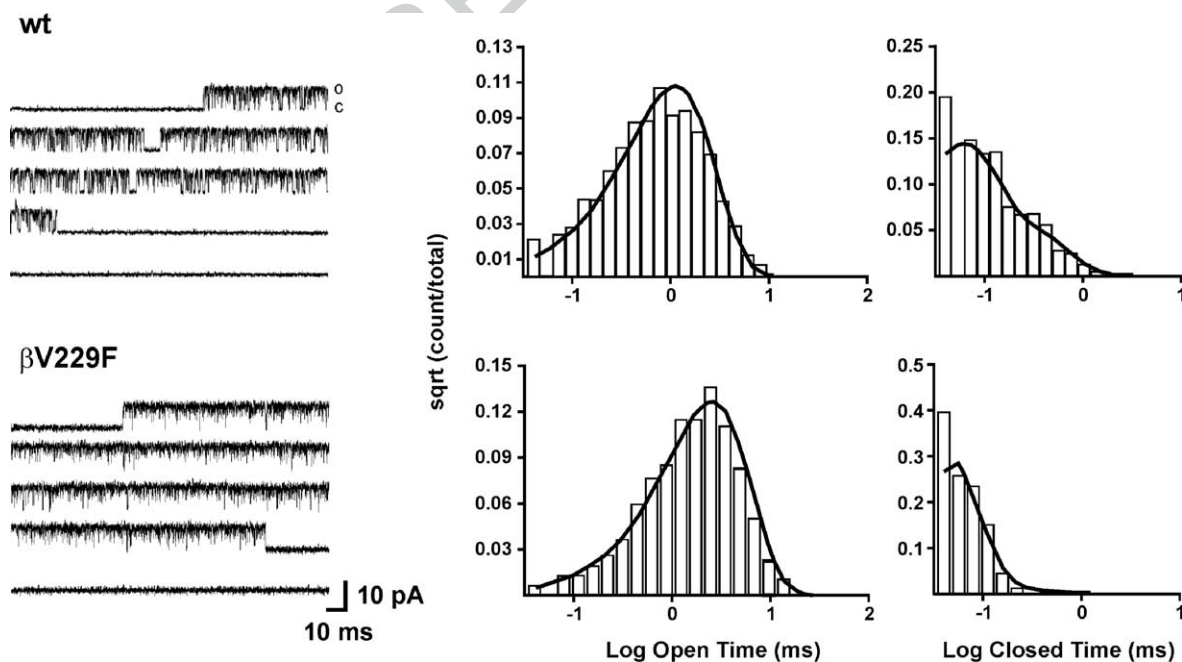


Fig. 5. Kinetic of activation of wild type and βV229F determined with $100 \mu\text{M}$ ACh. Currents were recorded from *Xenopus* oocytes expressing either wild-type or the mutant AChRs, as indicated. Corresponding histograms of open and closed durations with superimposed probability density functions for scheme 1 (see Experimental methods) of receptor activation at $100 \mu\text{M}$ ACh. Table 4 shows the fitted rate constants. Data were filtered at 5 kHz for each current sample displayed and channel openings shown as upward deflections (left side panel). Each current trace represents continuous single-channel current recordings corresponding to bursts of activity for each of the AChRs tested. All channels were recorded at a holding potential of -100 mV, sampling rate of 50 kHz and at a temperature of 22°C .

t5.1 Table 5

t5.2 Kinetic parameters of wt and mutant AChRs expressed in *Xenopus* oocytes

t5.3	AChR	Events	Bursts	τ_o (ms)	f	τ_c (ms)	f	k_{-2}	β_2	α_2	Θ_2	P_o
t5.4	wt	18,736	50	1.0	0.93	0.05	0.58	3600 ± 200	19,000 ± 400	1700 ± 25	11	0.86
t5.5	β V229F	25,986	77	1.6	0.91	0.03	0.94	700 ± 64	33,500 ± 300	1200 ± 16	28	0.96

Single-channel currents were recorded in cell-attached patches at a holding potential of -100 mV, temperature at 22°C and at a sampling rate of 50 kHz. Θ is the diliganded channel open equilibrium constant. This constant corresponded to ratios of opening and closing diliganded rate constants. Values are the result of fitting scheme 1 to the data obtained at 100 μM ACh. Rate constant are in s^{-1} .

t5.6

257 closing rate and the 2-fold increase in the effective channel opening
 258 rate increase the mean burst duration from 2.6 ms in wild-type to
 259 20.7 ms in the β V229F mutation. The increase in mean burst
 260 duration calculated from in vitro expression studies correlates well
 261 with the decay time constant calculated from MEPC observed in
 262 the patient (see Tables 1 and 4). The small difference between the
 263 mean burst duration and the decay time of the MEPC observed for
 264 the β V229F mutation can be due to an increase in channel
 265 desensitization produced by the continuous presence of the agonist
 266 in the recording pipette. Nevertheless, the increase in mean burst
 267 duration alone is sufficient to explain the prolonged MEPC
 268 observed in the patient.

269 Prolongation of synaptic currents leads to cation and particu-
 270 larly calcium overload, a stress that may ultimately reduce the
 271 amplitude of the MEPCs, by several mechanisms: (1) a decrease in
 272 the sodium driving force due to cation overload. This may also
 273 affect muscle fiber excitability by causing depolarization block of
 274 Na channels; (2) a reduction in the density of AChRs in the
 275 endplate because of reduced expression of AChR subunit genes;
 276 (3) activation of degradative enzymes leading to the degenerative

and remodeling changes of endplate myopathy (see below). In
 addition, mutant AChRs may have a greater tendency to
 desensitize, which would lead to further reduction of the MEPC
 amplitude (Milone et al., 1997). Finally, the observed 40%
 reduction in the quantal release could significantly reduce MEPCs
 in the patient. Future experiments using ultrastructural and
 electrophysiological studies in transgenic mouse models or
 biopsies of patients bearing this mutation should shed light into
 the exact mechanism responsible for reduce amplitude of the
 MEPC.

The pathological hallmark of the SCS is the endplate myopathy,
 seen only at the electron microscopic level. Endplate myopathy
 represents a combination of degenerative and remodeling changes
 of the neuromuscular junction that include widening of the
 synaptic cleft, degeneration or enlargement of synaptic folds and
 degeneration of subsynaptic nuclei and mitochondria. These
 changes have been attributed to overload of the subsynaptic region
 by cations, principally calcium (Engel et al., 1982; Gomez et al.,
 2002b). Previous observations have demonstrated that one patient
 from this kindred manifested a typical endplate myopathy that

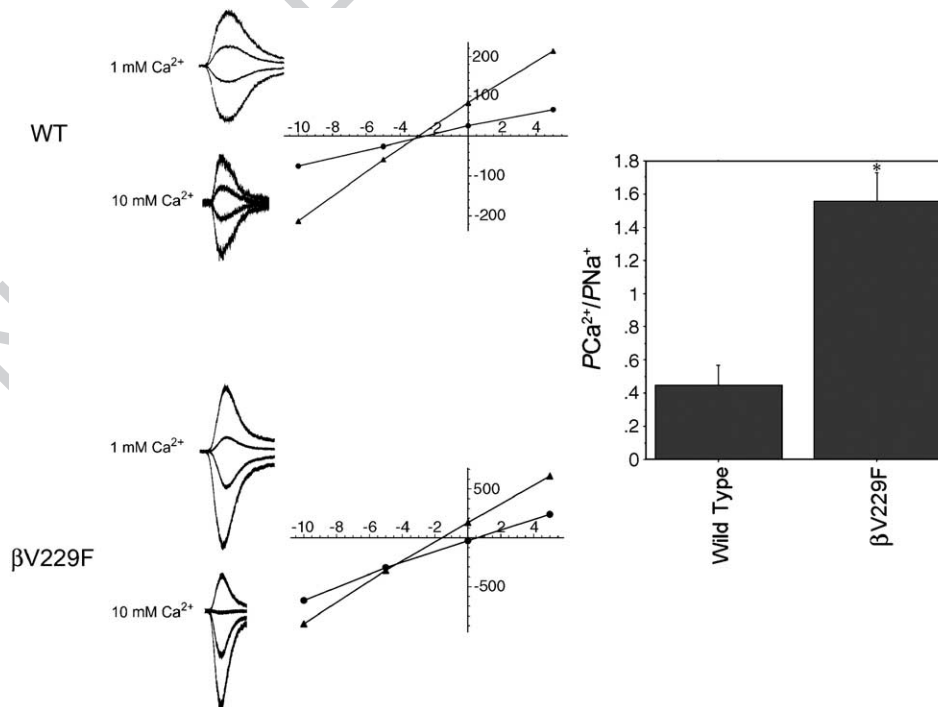


Fig. 6. M1 mutations in SCCMS differentially affect calcium permeability. (A) Whole-cell current traces elicited over a range of holding potentials (-10 mV to $+15$ mV, with 4 representative traces shown) in HEK-293 cells expressing AChRs bearing mutation β V229F in the presence of 1 mM (left) or 10 mM (right) Ca^{2+} . (B) Current–voltage relationships used to determine reversal potentials. (C) Relative permeability ($P_{\text{Ca}^{2+}}/P_{\text{Na}^+}$) for wild-type or β V229F AChRs computed using reversal potentials and an extended Goldman–Hodgkin–Huxley equation as described in Experimental methods. The value of $P_{\text{Ca}^{2+}}/P_{\text{Na}^+}$ obtained for β V229F AChRs, 1.56 ± 0.41 ($n = 6$), was significantly greater than that of wild type, 0.37 ± 0.24 ($n = 4$, $P < 0.001$, mean \pm SD).

297 included pronounced remodeling of the neuromuscular junctional
298 sarcoplasm (Gomez et al., 2002b). As with biopsies of other SCS
299 muscle, calcium deposits were occasionally detected at endplates
300 of this patient. Interestingly, our calcium permeation studies
301 indicate that mutation β V229F produced a significant increase in
302 relative calcium permeability (Fig. 6). This observation suggests
303 that an increase in the preference of the channel to conduct calcium
304 could be a factor contributing to the endplate myopathy observed
305 in the patient. Excessive intracellular calcium accumulation could
306 result in activation of harmful enzymatic and degradative protease
307 pathways that ultimately contribute to the pathology of the disease.
308 In support of this, we were able to demonstrate evidence of
309 deposition of activated caspase enzymes at endplates of this and
310 several SCS patients' muscles (Gomez et al., 2002b).

311 According to the predicted AChR structure (Miyazawa et al.,
312 2003), position β V229 is located in the upper third portion of the
313 M1 domain. Structural studies have suggested that, at the point
314 where the outer portion of the ion channel pore widens, the M2
315 domains of the five subunits cannot alone span the larger
316 circumference, implying that a portion of the M1 domain must
317 contribute to the lining of the ion channel (Akabas and Karlin,
318 1995). Substituted-cysteine-accessibility studies had shown that
319 position β V229 is accessible to solvent in the open state, but not in
320 the resting state of the channel, suggesting that this position
321 contributes to the lumen of the AChR in the open conformation
322 (Zhang and Karlin, 1997). Thus, the significant increase in the
323 preference of the receptor for using Ca^{2+} as a charge carrier in the
324 mutant AChR suggests that position β V229 not only contributes to
325 the formation of the ion channel pore, but is also involved in
326 determining the ion selectivity of the channel. In addition, our
327 results indicate that mutation β V229F either affects the diameter of
328 the permeation path, the net charge contributing to the driving
329 force or changed the Ca^{2+} binding regions of the pore region.

330 Comparison with other SCS mutations

331 To date, 15 different SCS mutations have been discovered in
332 the extracellular, M1 and M2 domains of the AChR (Engel et al.,
333 2003). The kinetic consequences of the SCS mutations vary
334 depending on its localization in the AChR. Accordingly, SCS
335 mutations in the extracellular domain near the acetylcholine
336 binding sites, such as α G153S, act mainly by increasing agonist-
337 binding affinity (Sine et al., 1995), while mutations in the M2
338 domain (α V249F, β V266M, ϵ L269F, among others) act mainly by
339 slowing down the closing rate constant of the active channel (Ohno
340 et al., 1995; Engel et al., 1996; Milone et al., 1997; Gomez et al.,
341 2002b). Unexpectedly, mutations in the M1 domain (α N217K and
342 ϵ L221F) have been shown to produce the kinetic abnormality
343 underlying the SCS mainly by reducing the agonist dissociation
344 rate constant (Wang et al., 1997; Croxen et al., 2002). These results
345 were surprising given the fact that the positions in which these
346 mutations are located are some 30 Å away from the agonist's
347 binding sites.

348 The mutation β V229F described in this study is similar to the
349 other SCS M1 domain mutations in that it reduces the agonist
350 dissociation constant and, as a consequence, increases the number
351 of openings per activation episode (Wang et al., 1997; Croxen
352 et al., 2002). The fact that a mutation in the M1 domain of the AChR
353 β subunit has such an effect on agonist-binding affinity is even
354 more surprising than the results obtained from previous SCS M1
355 domain mutations. The large effect on the agonist dissociation

constant for the diliganded channel observed for the α N217K and
 ϵ L221F mutations is consistent with the fact that the acetylcholine
binding sites are located in the interface between the α - δ and α - ϵ
subunits (Karlin, 2002). That is, it is not surprising that
perturbations caused by these mutations allosterically propagate
to the binding sites and affect agonist-binding affinity. Alternatively,
these mutations may be acting even closer by stabilizing the
interaction between residues involved in the principal pathway
coupling agonist binding to channel gating in the so-called pre-M1
domain region (Lee and Sine, 2005). However, given that the
AChR β subunit does not contribute to the formation of the
agonist-binding pockets, the structural and functional basis for the
produced effect of the β V229F mutation on the agonist dissociation
constant remains obscure. The development of a high-resolution
crystal structure of the acetylcholine receptor in the different
conformational states should help clarify this issue.

Unlike the other SCS M1 domain mutations, the β V229F
mutation significantly affects the parameters governing channel
gating. It produces a substantial increase in the effective channel
opening rate and a reduction in the channel closing rate. Perhaps,
the bigger, more hydrophobic phenylalanine substitution enhances
gating by creating new interactions with residues in the nearby M2
domain. The perturbation produced by the mutation will then
propagate to the proposed channel gate region during channel
activation only a couple of amino acids below. Nevertheless, our
results indicated a modulatory role of the M1 domain in structures
that couple ligand binding to the channel gate.

To summarize, we found that the clinical and electrophysiological
outcome of a novel form of the SCS is caused by a β V229F
mutation in the M1 domain of the AChR β subunit. The kinetic
and permeation studies presented in this work help to explain the
consequences of the β V229F mutation on the miniature endplate
currents and thus are direct evidence that the β V229F mutation is
responsible for compromising the safety margin of neuromuscular
transmission in the patient. Furthermore, our results indicated a
contribution of position β V229 to channel gating and an apparent
allosteric modulation of the binding site. These results highlight the
importance of understanding the conformational changes and
molecular interaction taking place during the process of agonist
binding to channel gating and their contribution to the shape of the
synaptic current.

Experimental methods

Genetic analysis of AChR subunit genes

Screening for mutations in the AChR α , β , δ and ϵ subunit genes was
carried out by direct sequence analysis of AChR subunit exons amplified
from genomic DNA by polymerase chain reaction (PCR) as described
previously (Gomez et al., 1995; Gomez et al., 1996, 2002a). Briefly,
primers corresponding to flanking intron sequences (sometimes containing
universal 5' M13 tail sequence) were used to amplify DNA templates for
nucleotide sequence analysis. Di-deoxy sequence analysis was carried out
using AChR-specific primers or M13 universal primer and analyzed on an
automated DNA sequencer (ABI 377, Applied Biosystems). The nucleotide
sequence of the entire coding region for the four AChR subunits was
determined after the mutations were identified to exclude the presence of
additional mutations. To screen for the presence of the nucleotide
substitution (β G770T) that codes for the β V229F mutation in a panel of
one hundred normal individuals from a DNA panel (Centre d'Etude du
Polymorphisme Humain), we used allele-specific PCR with upstream
primer β 7U (CAT.ACC.CGG.CAC.TAA.CCA.GG), the downstream primers
 β 7D (GGA.TGC.ATG.GGG.CAA.TGA.c) and β 7Dm (GGA.TG-

416 C.ATG.GGG.CAA.TGA.a), which give 24-bp PCR products for wild-type
417 and mutant alleles, respectively.

418 *Oocyte expression studies*

419 The homologous β V229F mutation was generated in mouse β subunit
420 cDNA cloned into the vector, pcDNA/3 using site-directed mutagenesis
421 (Quick-change, Stratagene, La Jolla, CA). The mutation was confirmed by
422 di-deoxy nucleotide sequence analysis of the entire cDNA. In vitro mRNA
423 transcription was performed as described previously (Gomez et al.,
424 2002a,b).

425 *Cell culture and transfection*

426 For reversal potential studies, human embryonic kidney 293 (HEK-293,
427 Gibco BRL, Carlsbad, CA) cells were maintained in culture at 37°C, 5%
428 CO₂ in DMEM containing 10% FBS and 0.05 mg/ml Gentamicin (Gibco
429 BRL, Carlsbad, CA). Cells were transfected at ~50% confluency using the
430 Effectene transfection reagent (Qiagen, Valencia, CA). For a 25-ml flask, a
431 total amount of 1 μ g of DNA was used, the transfection mix was composed
432 of a ratio of 2 α : β : ϵ : δ subunits. Cells expressing mature receptors were
433 selected 36–48 h after transfection by using magnetic beads (Dynal
434 Biotech, Lake Success, NY) coated with the mAb35 antibody (Tzartos and
435 Lindstrom, 1980). Cells were replated into 60-mm petri dishes, and
436 recordings were performed 18–24 h after replating.

437 *Voltage clamp recordings*

438 ACh-induced currents were recorded with two-electrode voltage clamp
439 3 days after mRNA injection with the Gene Clamp 500 amplifier (Axon
440 Instruments, Foster City, CA). Electrodes were filled with 3 M KCl and had
441 resistances of less than 2 M Ω . Impaled oocytes in the recording chamber
442 were perfused at a rate of 0.5 ml/s with MOR-2 buffer [82 mM NaCl, 2.5
443 mM KCl, 5 mM MgCl₂, 1 mM Na₂HPO₄, 5 mM N-(2-Hydroxyethyl)pi-
444 perazine-N'-2-ethanesulfonic acid (HEPES) and 0.2 mM CaCl₂ (pH 7.4)].
445 Dose–response curves for each oocyte were held at a membrane potential
446 of –70 mV. Dose–response data were collected and analyzed as described
447 previously (Tamamizu et al., 1999).

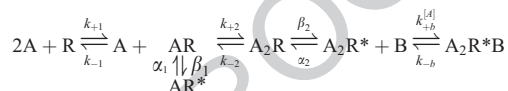
448 [¹²⁵I]- α -Bungarotoxin binding assay

449 The expression of nAChR in the oocyte membrane was assayed by
450 assessing the binding of [¹²⁵I]- α -bungarotoxin (¹²⁵I- α BT) (Amersham Life
451 Sciences, Arlington Heights, IL) to intact oocytes as described previously
452 (Tamamizu et al., 1999).

453 *Single-channel recordings*

454 *Xenopus* oocytes were placed in a recording chamber containing a bath
455 solution of 100 mM KCl, 1 mM MgCl₂ and 10 mM HEPES (pH 7.2) at 20 to
456 22°C. The patch pipettes were made of thick-walled borosilicate glass
457 (Sutter Instruments, Novato, CA). Pipettes typically had resistance of 2–4
458 M Ω . The pipette solution contained 100 mM KCl, 10 mM HEPES, 10 mM
459 EGTA (pH 7.2) and 4 or 100 μ M ACh. All experiments were performed in
460 the cell-attached configuration at a membrane potential of –100 mV (Hamill
461 et al., 1981). Single-channel currents were recorded using an Axopatch
462 200B patch clamp amplifier (Axon Instruments), filtered at 5 kHz and stored
463 on VHS tapes using a digital data recorder (VR-10B, Instrutech Corp.,
464 Mineola, NY). The data traces were played back into a Pentium-III-based
465 computer through a DigiData 1200 interface (Axon Instruments) and
466 digitalized at 50 kHz using the program Fetchex (Axon Instruments). Single-
467 channel events at low ACh concentration (4 μ M) were detected with a half-
468 amplitude crossing algorithm (pClamp6). Open and closed time duration
469 distributions were constructed from pClamp6-generated files using a
470 logarithmic abscissa and a squared root ordinate (Sigworth and Sine,
471 1987) and fitted using the maximum likelihood algorithm with the
472 appropriate number of components using the program pSTAT (Axon

Instruments). At 100 μ M ACh concentration, all the channels in the pipette
473 are desensitized. However, individual receptors randomly revert to the non-
474 desensitized state and the kinetic behavior of the opened and closed states of
475 only one channel can be measured as a burst of activity. A burst of openings
476 corresponding to a single channel was defined as a series of openings
477 separated by closed intervals greater than some critical duration (τ_{crit}). This
478 duration was taken as the point of intersection of the predominant closed
479 component and the succeeding one in the closed time histogram, as
480 described elsewhere (Bouzat et al., 2000). Single-channel events at 100 μ M
481 ACh concentration were detected and idealized with a half-amplitude
482 crossing criterion using the program QUB (QUB suite, State University of
483 New York, Buffalo). Only bursts that exhibited durations longer than 100 ms
484 and more than 10 openings per burst were used for further analysis. The
485 resulting open and closed time intervals from single patches at 100 μ M ACh
486 were analyzed according to the following kinetic scheme using the program
487 MIL (QUB suite, State University of New York, Buffalo). 488



In this scheme, R is the receptor, A is ACh, A₂R is the bi-liganded
490 species, AR* and A₂R* are the mono-liganded and bi-liganded open state
492 of the receptor–ligand complex, respectively, B is the block molecule and
493 A₂R* is the blocked state of the channel. k_{+1} and k_{+2} are the binding rate
494 constants and k_{-1} and k_{-2} the first and second dissociation rate constants
495 for the first and second site, respectively. α_1 and α_2 are the fast and slow
496 closing rate constants, respectively, and β_1 and β_2 are the open rate
497 constants, respectively. k_{+b} is the blocking rate and k_{-b} is the rate of
498 opening from the blocked state. The dead time used was set to 30 μ s.
499 Probability density functions of open and closed durations were calculated
500 from the fitted rate constants and superimposed on the experimental dwell-
501 time histograms (Qin et al., 1996). 502

503 *Calcium permeability*

Recordings from HEK-293 cells were obtained in whole cell
504 configuration with an Axoclamp 200B amplifier and digitized through a
505 Digidata 1320A (Axon Instruments) at 22–23°C. Patch electrodes were as
506 above except with resistances of 2–4 M Ω . The electrode solution was
507 composed of 145 mM CsCl, 10 mM HEPES and 5 mM 1,2-bis(2-
508 aminophenoxy)ethane-N,N,N',N'-tetra acetate (pH 7.3). Recordings were
509 initiated in extracellular solution containing 150 mM CsCl, 1 mM CaCl₂
510 and 10 mM HEPES (pH 7.3). To determine the reversal potential of the
511 AChRs voltage, ramp protocols were applied while a fast step perfusion
512 system (Warner Instruments, Hamden, CT) applied an extracellular solution
513 containing 100 μ M ACh. This protocol was succeeded by repeating the
514 ramp protocol with a solution containing 100 μ M ACh. The data were
515 acquired using the pClamp 8 software (Axon Instruments) in a Pentium III
516 personal computer. The value of the reversal potential was determined for
517 the different mutations at 1 mM and 10 mM CaCl₂. The calcium
518 permeability was determined by using an extended GHK equation used
519 to calculate the relative ion permeabilities with respect to Cs⁺ (Castro and
520 Albuquerque, 1995): 521

$$\frac{P_{Ca}}{P_{Cs}} = \frac{[Cs^+]_o(1 - e^{\Delta V_{rev}F/RT})}{4[Ca^{2+}]_o e^{\Delta V_{rev}F/RT}(1 + e^{\Delta V_{rev}F/RT})^{-1} - 4[Ca^{2+}]_o(1 + e^{\Delta V_{rev}F/RT})^{-1}}$$

Permeability calculations were made using the Mathematica 4.1
524 (Wolfram Research Inc, Champaign, IL) software. Statistical analyses of
525 these results were made using the StatView (SAS institute Inc, Cary NC)
526 software package. 527

528 *Acknowledgments*

This work was supported by grant RO1 NS33202, RO1
529 NS36809 (to CMG), S06-GM50695 (to LVR) and RO1
530 GM56371-5 and GM08102-27 (to JALD). Manuel Navedo was
531

532 supported by NIH-MBRS Research Initiative to Support Excel-
533 lence 5R25GM61151), Carlos A. Báez-Pagán was supported by
534 the UPR-AGEP Grant (HDR981746), Luzed Díaz-Pérez by the
535 LSAMP program (NSFHRD-0114586) and Roberto Zayas was
536 supported by Supplement award R01 NS33202-0S1.

537 References

538

- 539 Akabas, M.H., Karlin, A., 1995. Identification of acetylcholine receptor
540 channel-lining residues in the M1 segment of the alpha-subunit.
541 *Biochemistry* 34, 12496–12500.
- 542 Bouzat, C., Barrantes, F.J., Sine, S.M., 2000. Nicotinic receptor
543 fourth transmembrane domain: hydrogen bonding by conserved
544 threonine contributes to channel gating kinetics. *J. Gen. Physiol.*
545 115, 663–672.
- 546 Burzomato, V., Beato, M., Groot-Kormlink, P.J., Colquhoun, D., Sivilotti,
547 L.G., 2004. *J. Neurosci.* 24, 10924–10940.
- 548 Castro, N.G., Albuquerque, E.X., 1995. Alpha-bungarotoxin-sensitive
549 hippocampal nicotinic receptor channel has a high calcium permeability.
550 *Biophys. J.* 68, 516–524.
- 551 Cens, T., Nargeot, J., Charnet, P., 1997. Ca²⁺-permeability of muscle
552 nicotinic acetylcholine receptor is increased by expression of the epsilon
553 subunit. *Receptor. Channels* 5, 29–40.
- 554 Colquhoun, D., 1998. Binding, gating, affinity and efficacy: the interpre-
555 tation of structure–activity relationships for agonists and of the effects
556 of mutating receptors. *Br. J. Pharmacol.* 125, 924–947.
- 557 Croxen, R., Newland, C., Beeson, D., Oosterhuis, H., Chauplannaz, G.,
558 Vincent, A., Newsom-Davis, J., 1997. Mutations in different functional
559 domains of the human muscle acetylcholine receptor alpha subunit in
560 patients with the slow-channel congenital myasthenic syndrome. *Hum.*
561 *Mol. Genet.* 6, 767–774.
- 562 Croxen, R., Hatton, C., Shelley, C., Brydson, M., Chauplannaz, G.,
563 Oosterhuis, H., Vincent, A., Newsom-Davis, J., Colquhoun, D.,
564 Beeson, D., 2002. Recessive inheritance and variable penetrance
565 of slow-channel congenital myasthenic syndromes. *Neurology* 59,
566 162–168.
- 567 Engel, A.G., Lambert, E.H., Mulder, D.M., Torres, C.F., Sahashi, K.,
568 Bertorini, T.E., Whitaker, J.N., 1982. A newly recognized congenital
569 myasthenic syndrome attributed to a prolonged open time of the
570 acetylcholine-induced ion channel. *Ann. Neurol.* 11, 553–569.
- 571 Engel, A.G., Ohno, K., Milone, M., Wang, H.L., Nakano, S., Bouzat, C.,
572 Pruitt, J.N., Hutchinson, D.O., Brengman, J.M., Bren, N., Sieb, J.P.,
573 Sine, S.M., 1996. New mutations in acetylcholine receptor subunit
574 genes reveal heterogeneity in the slow-channel congenital myasthenic
575 syndrome. *Hum. Mol. Genet.* 5, 1217–1227.
- 576 Engel, A.G., Ohno, K., Sine, S.M., 2003. Sleuthing molecular targets for
577 neuromuscular diseases at the neuromuscular junction. *Nat. Rev.* 4,
578 339–352.
- 579 Gomez, C.M., Gammack, J.T., 1995. A leucine-to-phenylalanine substitu-
580 tion in the acetylcholine receptor ion channel in a family with the slow-
581 channel syndrome. *Neurology* 45, 982–985.
- 582 Gomez, C.M., Ricardo Maselli, B.S., Lasalde, J., Tamamizu, S., Cornblath,
583 D.R., Lehar, M., McNamee, M., Kuncl, R.W., 1996. A β subunit
584 mutation in the acetylcholine receptor channel gate causes severe slow-
585 channel syndrome. *Ann. Neurol.* 39, 717–723.
- 586 Gomez, C., Staub, J., Maselli, R., Day, J., Charnet, P., Cens, T., Wollmann,
587 R., 1998. Novel β and δ subunit acetylcholine receptor mutations in the
588 slow-channel syndrome demonstrate phenotypic variability. *Society for*
589 *Neuroscience Abstracts.* (Los Angeles, CA).
- Gomez, C., Maselli, R., Vohra, B., Navedo, M., Stiles, J., Charnet, P., 590
Schott, K., Rojas, L., Keeseey, J., Verity, A., Wollmann, R., Lasalde- 591
Dominicci, J., 2002a. Novel delta subunit mutation in slow-channel 592
syndrome causes severe weakness by novel mechanisms. *Ann. Neurol.* 593
51, 102–112. 594
- Gomez, C.C., Maselli, R., Groshong, J., Zayas, R., Wollman, R.L., Cens, 595
T., Charnet, P., 2002b. Active calcium accumulation underlies severe 596
weakness in a panel of mice with slow-channel syndrome. *J. Neurosci.* 597
22, 6447–6457. 598
- Hamill, O.P., Marty, A., Neher, E., Sakmann, B., Sigworth, F.J., 1981. 599
Improved patch-clamp techniques for high-resolution current record- 600
ing from cells and cell-free membrane patches. *Pflugers Arch.* 391, 601
85–100. 602
- Hatton, C.J., Shelley, C., Brydson, M., Beeson, D., Colquhoun, D., 2003. 603
Properties of the human nicotinic receptor, and of the slow-channel 604
myasthenic syndrome mutant ϵ L221F, inferred from maximum likeli- 605
hood fits. *J. Physiol.* 547, 729–760. 606
- Karlin, A., 2002. Emerging structure of the nicotinic acetylcholine 607
receptors. *Nat. Rev., Neurosci.* 3, 102–114. 608
- Lee, W.Y., Sine, S.M., 2005. Principal pathway coupling agonist binding to 609
channel gating in nicotinic receptors. *Nature* 438, 243–247. 610
- Milone, M., Wang, H.L., Ohno, K., Fukudome, T., Pruitt, J.N., Bren, N., 611
Sine, S.M., Engel, A.G., 1997. Slow-channel myasthenic syndrome 612
caused by enhanced activation, desensitization, and agonist binding 613
affinity attributable to mutation in the M2 domain of the acetylcholine 614
receptor alpha subunit. *J. Neurosci.* 17, 5651–5665. 615
- Miyazawa, A., Fujiyoshi, Y., Unwin, N., 2003. Structure and gating 616
mechanism of the acetylcholine receptor pore. *Nature* 424, 949–955. 617
- Muley, S., Gomez, C., 2002. Congenital myasthenic syndromes. In: 618
Kaminski, H. (Ed.), *Disorders of the Neuromuscular Junction.* Humana 619
Press. 620
- Ohno, K., Hutchinson, D., Milone, M., Brengman, J., Bouzat, C., Sine, S., 621
Engel, A., 1995. Congenital myasthenic syndrome caused by prolonged 622
acetylcholine receptor channel openings due to a mutation in the M2 623
domain of the ϵ subunit. *Proc. Natl. Acad. Sci.* 92, 758–762. 624
- Qin, F., Auerbach, A., Sachs, F., 1996. Estimating single-channel kinetic 625
parameters from idealized patch-clamp data containing missed events. 626
Biophys. J. 70, 264–280. 627
- Sigworth, F.J., Sine, S.M., 1987. Data transformations for improved display 628
and fitting of single channel dwell time histograms. *Biophys. J.* 52, 629
1047–1054. 630
- Sine, S.M., Ohno, K., Bouzat, C., Auerbach, A., Milone, M., Pruitt, J.N., 631
Engel, A.G., 1995. Mutation of the acetylcholine receptor α subunit 632
causes a slow-channel myasthenic syndrome by enhancing agonist 633
binding affinity. *Neuron* 15, 229–239. 634
- Tamamizu, S., Lee, Y., Hung, B., McNamee, M.G., Lasalde-Dominicci, 635
J.A., 1999. Alteration in ion channel function of mouse nicotinic 636
acetylcholine receptor by mutations in the M4 transmembrane domain. 637
J. Membr. Biol. 170, 157–164. 638
- Tzartos, S.J., Lindstrom, J.M., 1980. Monoclonal antibodies used to probe 639
acetylcholine receptor structure: localization of the main immunogenic 640
region and detection of similarities between subunits. *Proc. Natl. Acad.* 641
Sci. U. S. A. 77, 755–759. 642
- Wang, H.L., Auerbach, A., Bren, N., Ohno, K., Engel, A.G., Sine, S.M., 643
1997. Mutation in the M1 domain of the acetylcholine receptor alpha 644
subunit decreases the rate of agonist dissociation. *J. Gen. Physiol.* 109, 645
757–766. 646
- Zhang, H., Karlin, A., 1997. Identification of acetylcholine receptor 647
channel-lining residues in the M1 segment of the beta-subunit. 648
Biochemistry 36, 15856–15864. 649